Characterization of nitrogen-containing radical products from the photodissociation of trimethylamine using photoionization detection

Nancy R. Forde[a)] and Laurie J. Butler
The James Franck Institute and Department of Chemistry, University of Chicago, Chicago, Illinois 60637

Branko Ruscic
Chemistry Division, Argonne National Laboratory, Argonne, Illinois 60439

Osman Sorkhabi, Fei Qi, and Arthur Suits
Chemical Sciences Division, Lawrence Berkeley National Laboratory, Berkeley, California 94720
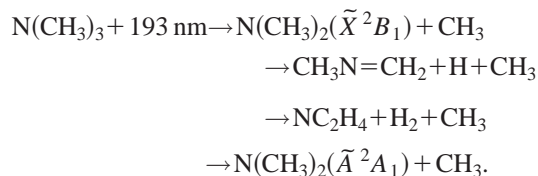
The outcome of neutral and photoionized $N(CH_3)_2$ primary products of trimethylamine photodissociation at 193 nm is determined by combining photoionization detection with supporting G3 theoretical calculations. $N(CH_3)_2$ primary products with very little internal energy show an experimentally observed ionization onset of 9.1 ± 0.2 eV, but do not appear at the parent ion ($m/e = 44$). Instead, the parent ion is unstable and easily fragments to $m/e = 42$, where the signal is observed. $N(CH_3)_2$ radicals with higher internal energies undergo H-atom loss from the neutral to give CH_2NCH_3, which has an observed ionization onset at parent ($m/e = 43$) of <9.3 eV. At slightly higher ionization energies, these secondary products also appear at $m/e = 42$ (where their appearance energy is roughly 9.8–9.9 eV, uncorrected for internal energy). Finally, $N(CH_3)_2$ radicals with the highest internal energy in this study appear to undergo H_2 loss as neutrals, giving rise to a species whose parent ion has $m/e = 42$. The ionization onset of this species at $m/e = 42$ is found to be in the range of 9.5–9.6 eV. © *2000 American Institute of Physics.* [S0021-9606(00)01332-5]

I. INTRODUCTION

We recently reported the results of the photodissociation reactions of trimethylamine $[N(CH_3)_3]$ following 193 nm excitation.[1] In analyzing the resulting dissociation pathways, we discovered that little is known about the energetics and ionization characteristics of methylated nitrogen-containing radicals. These radicals were of interest to us both as products of the photodissociation reactions of trimethylamine[1] and dimethylformamide[2,3] at 193 nm, and also as possible participants in combustion reactions. The experiments outlined in this paper seek to characterize the methylated nitrogen-containing products of the photodissociation of trimethylamine at 193 nm, by analyzing both their energetics and ionization properties.

Nitrogen-methyl bond fission was the only primary photodissociation pathway identified following 193 nm excitation of trimethylamine.[1] The primary $N(CH_3)_2$ radical products were found to exhibit distinct ionization characteristics depending on their internal energy (given by the 193 nm photon energy minus the $N-CH_3$ bond energy and observed translational energy). This suggested the existence of additional channels, possibly proceeding through secondary dissociation of the neutral species and/or competitive fission to electronically excited $N(CH_3)_2$ ($\tilde{A}\,^2A_1$) radicals. Several possibilities were considered:

$$N(CH_3)_3 + 193\,nm \rightarrow N(CH_3)_2(\tilde{X}\,^2B_1) + CH_3$$
$$\rightarrow CH_3N{=}CH_2 + H + CH_3$$
$$\rightarrow NC_2H_4 + H_2 + CH_3$$
$$\rightarrow N(CH_3)_2(\tilde{A}\,^2A_1) + CH_3.$$

Based on theoretical estimates of its energy,[3,4] the formation of $N(CH_3)_2(\tilde{A}\,^2A_1)$ was discounted as a primary reaction product.[1] To distinguish among the remaining possible channels, information such as the energies of formation and ionization are needed for the products of the secondary dissociation reactions. Table I summarizes these values available from the few earlier studies found in the literature.[5–21] Studies on the neutral species of formula NC_2H_4 are particularly scant, and various possibilities exist for its structure, including the linear $HCNCH_3$ and H_2CNCH_2 forms.

This study provides a characterization of both the $N(CH_3)_2$ radical and its secondary neutral and ionic dissociation channels by using the photodissociation of trimethylamine at 193 nm as a primary radical source, and tunable photoionization to detect the primary and secondary neutral photofragments. Tunable photoionization, at least in principle, permits sensitive detection of reaction products just above their threshold for ionization, which, by reducing the excess internal energy of the parent ions, eliminates or significantly reduces dissociative ionization channels that complicate other detection techniques.[1] Besides obtaining information on the ionization energies of the reaction products, the amount of internal energy in the primary $N(CH_3)_2$ prod-

_____

[a)]Electronic mail: nforde@alice.berkeley.edu

J. Chem. Phys., Vol. 113, No. 8, 22 August 2000

Photodissociation of trimethylamine   3089

TABLE I. Literature values for the experimental enthalpies of the formation and ionization energies of several species of interest in this paper.

Species	$\Delta H^0_{f,298}$ (kcal/mol)	Ionization energy (eV)
$N(CH_3)_3$	-5.67 ± 0.18 (Refs. 5, 6)	$7.76 - 8.56$ (Ref. 5)
		7.85 ± 0.05 (eval.) (Ref. 5)
$CH_2N(CH_3)_2$	31.1 ± 2.4 (Ref. 7)[a]	
$N(CH_3)_2$	$\leqslant 30.3$ (Ref. 8)	5.17 (Ref. 5)
	33.7 (Ref. 9)	$<9.42 \pm 0.1$ (Ref. 8)
	33.8 ± 3 (Ref. 10)[b]	9.01 ± 0.02 eV (Ref. 20)[c]
	34 (Refs. 11, 12)	
	35 ± 2 (Ref. 13)	
	39 (Ref. 14)	
	29.3 ± 2 (Ref. 15)	
	37.4 (Ref. 16)	
	38.2 (Ref. 17)	
CH_2NCH_3	11 ± 2 (Refs. 5, 18)	adiabatic:
		$9.3, 9.4, 9.8 \pm 0.1$ (Ref. 5)
		vertical:
		$10.0, 9.90 \pm 0.02$ (Ref. 5)
CH_2NCH_2	63 ± 3 (Ref. 19)	

[a]The value in Ref. 7 is for the bond dissociation energy of $N(CH_3)_3 \rightarrow CH_2N(CH_3)_2 + H$. We have used the values (Ref. 5) of ΔH^0_f for $N(CH_3)_3$ and H to determine an estimated ΔH^0_f for $CH_2N(CH_3)_2$.

[b]The published value for ΔH^0_f of $N(CH_3)_2$ and bond enthalpies in Ref. 10 are in error by 0.9 kcal/mol (Ref. 21), and so we have made the appropriate correction here.

[c]A photoelectron value, not necessarily implying that the parent ion is stable.

ucts can also be determined, by analyzing the amount of energy disposed to relative product translation of the $N(CH_3)_2 + CH_3$ products. In this paper we present the experimentally determined limits on the enthalpies of the formation and ionization energies of the resulting nitrogen-containing radicals and closed-shell species. By combining these results with theoretical calculations, we have characterized secondary dissociation channels of the $N(CH_3)_2$ radical photoproduct, providing a deeper understanding of the complicated dynamics at play in these nitrogen-containing systems.

II. EXPERIMENTAL DETAILS

These experiments studied the photodissociation products of trimethylamine at 193 nm by detecting the neutral photofragment recoil distributions with a crossed laser–molecular beam apparatus, described in detail in Ref. 22. Tunable photons employed for the product detection via photoionization were produced when the ALS electron beam passed through a U10 undulator (bandwidth at FWHM=0.5 eV).[23,24] Various filtering methods were used to eliminate higher harmonics of the selected energy. Unless otherwise noted, the experiments described in this paper used a probe photon energy of 10.5 eV with a MgF_2 window in place to eliminate virtually all photon flux above 11 eV.

A 5% mixture of trimethylamine [$N(CH_3)_3$] in helium (obtained from Matheson Gas Products) was expanded from the pulsed valve source (nozzle diameter=1 mm), with a stagnation pressure of 500 Torr. A scan of the mass spectrum in the range from monomer to dimer mass/charge ratio under typical experimental conditions revealed no contributions from species of higher mass than monomer. The intensity of
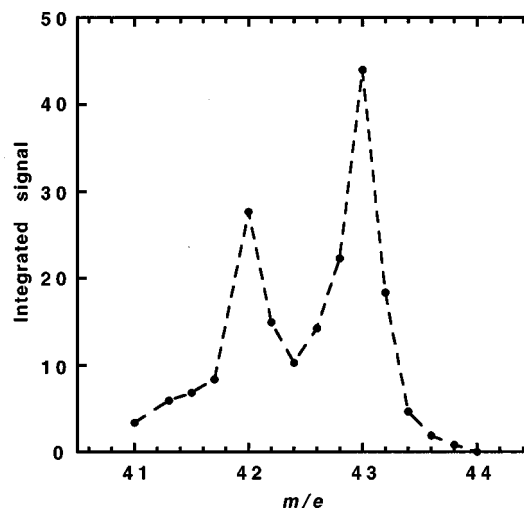

FIG. 1. Mass spectral sweep of photofragments at 10.5 eV over the range from $m/e = 42-44$, showing that there are peaks at $m/e = 42$ and $m/e = 43$, but that the signal decreases monotonically past $m/e = 43$ to $m/e = 44$. There is no evidence for the parent $N(CH_3)_2^+$ ion signal at $m/e = 44$.

the parent $N(CH_3)_3^+$ ion signal was, however, strongly dependent on ionization energy through the range of 9–12.7 eV. The ionization potential of trimethylamine is 7.85 eV,[5] and for probe photon energies below 10 eV, the signal at parent ($m/e = 59$) was much stronger than the signal at $m/e = 58$. At higher ionization energies, however, the parent peak diminished in intensity as dissociative ionization became competitive, such that at 12.7 eV, the peak at $m/e = 58$ was much more intense than the parent peak. The molecular beam was characterized via hole burning at the parent ion ($m/e = 59$) at either 10 or 10.5 eV, with the mean peak beam velocity found to be 1.30×10^5 cm/s and a full width at half-maximum (FWHM) of 35%.

In the experiments described here, we have measured the signal for several parent and daughter ions of the neutral photoproducts at various angles of the molecular beam with respect to the detector axis: at $m/e = 43$ (10°, 11 eV; 30°, 11 eV), 42 (30°, 10 eV; 30°, 10.5 eV; 30°, 11 eV) and 15 (30°, 10.5 eV; 50°, 10.5 eV). No discernible signal was observed at $m/e = 57$ (10°, 10.5 eV), 30 (10°, 10.5 eV), 29 (10°, 10.5 eV), 17 (30°, 10.5 eV) or 16 (10°, 13.5 eV). The quadrupole was adjusted to approximately 0.4 amu resolution (FWHM).

In addition, a very small signal was observed at $m/e = 44$ (10°, 10 eV; 10°, 10.5 eV; 30°, 10.5 eV). In order to determine the source of this signal, photofragment TOF spectra were collected at 0.2 amu intervals from $m/e = 42.0$ to 44.0 (30°, 10.5 eV). Because this signal is observed off the molecular beam (center-of-mass) velocity axis, it arises from photoproducts. One can determine the source of this signal by integrating the area under the photofragment TOF spectrum as a function of the mass/charge ratio of the ions passing through the quadrupole mass filter. The resulting integrated peak intensities (see Fig. 1) show that, while photoproducts appear at $m/e = 42$ and 43 (with clear separation of the masses by the quadrupole), no $m/e = 44$ can be discerned above the very small high-mass wing of $m/e = 43$. In addition, the photoionization curves constructed

from data collected nominally at $m/e = 44$ appeared identical to those obtained for the $m/e = 43$ signal. This places an upper limit on the possible intensity of the signal at $m/e = 44$ as $< 10^{-3}$ of the intensity at $m/e = 43$.

We determined the photoionization yields for the photoproduct signal at $m/e = 42$ and 43 by recording TOF spectra at each mass. The spectra were collected at 0.2 eV increments of the nominal photon energy from 8.7–10.7 eV ($m/e = 42$) and from 8.5–10.7 eV ($m/e = 43$), for 50 000 laser shots, each with a 30° angle between the molecular beam and detector axes. The MgF$_2$ window was in place for all of these scans, and the laser power was held constant at 55 mJ/pulse. The integrated peak area for each species was corrected for drift in the probe photon flux and was plotted as a function of photoionization energy.

A power study of the observed TOF signal was the most direct way to ensure that the electronic transition of trimethylamine was not saturated. (The ArF excimer transition provided the 193 nm light.) We conducted a power study of the signal at $m/e = 42$ with laser powers ranging from 10 to 60 mJ/pulse, resulting in attenuated powers of roughly 80% in the interaction region, a cross-sectional area of 1×3 mm^2. It revealed no change to the fast edge of the TOF spectrum, and so the experiments described in this chapter were run with a laser power of between 50–60 mJ/pulse, at 100 Hz repetition rates.

III. THEORETICAL METHODOLOGY

Supporting calculations were performed using the GAUSSIAN 98 package of programs,[25] with the intent of providing insight into the possible dissociation and ionization channels of relevance to these experiments. As shown previously,[7,26–34] the potential energy surfaces of the species NC$_n$H$_m$ and particularly the ions NC$_n$H$_m^+$ are quite complex, exhibiting a large number of minima and saddle points, corresponding to a considerable number of isomers and conformers. From these possible species, a relevant subset was chosen, and calculations of bond dissociation energies, ionization energies, and fragment appearance energies (corresponding to dissociative ionization) were performed, to enable the determination of the ionic and neutral species formed in the present experiments.

Calculations leading to thermochemical quantities presented in Table II (and in Tables III–V of Ref. 35) were performed at the G3 level of theory,[36] which is the latest in the series of Gaussian-n theories. Using the G2/97 test set, the reported overall average absolute deviation between experiment and the G3 results is 1.02 kcal/mol, corresponding to a standard deviation $\sigma = 1.47$ kcal/mol. Hence, for the species considered in the present work, the G3 calculated results are expected to fall within ± 3 kcal/mol of the true value. More details of the calculations performed here are found in the electronic supplementary material (EPAPS).[35]

IV. RESULTS AND ANALYSIS

The photofragment TOF spectra from these experiments are consistent with the results of earlier experiments, showing N–CH$_3$ bond fission to be the dominant primary disso-

TABLE II. Calculated ionization energies and fragment appearance energies of interest to the present study. All values are at the G3 level of theory. IE$_a$ and IE$_v$ refer to the adiabatic and vertical ionization energies, respectively, while AE$_0[AB^+/ABC]$ is the 0 K appearance energy of the AB^+ ionic fragment formed by the photoionization process $ABC + h\nu \rightarrow AB^+ + C + e^-$.

Quantity	Calculated value (eV)
IE$_a$[N(CH$_3$)$_3$]	7.87
IE$_a$[H$_3$C–N–CH$_3$] to ^1A cation	9.05
IE$_v$[H$_3$C–N–CH$_3$] to singlet surface	9.68
IE$_a$[H$_3$C–N–CH$_3$] to $^3B_1$ cation	8.97
IE$_v$[H$_3$C–N–CH$_3$] to triplet surface	9.82
IE$_a$[H$_3$C–N–CH$_3$] to $^1A'$ ring cation	6.19
IE$_a$[H$_3$C–N–CH$_3$] to $^1A'$ (C_s)CH$_2$NHCH$_3^+$ cation	5.72
AE$_0$[CH$_2$NHCH$_3^+$, $^1A'(C_s)$/N(CH$_3$)$_3$]	9.08
AE$_0$[CH$_2$NHCH$_3^+$, $^1A'(C_s)$/NH(CH$_3$)$_2$]	9.73
IE$_a$[H$_3$C–N–CH$_2$] to $^2A'$ H$_3$C–N–CH$_2^+$ cation	9.14
IE$_v$[H$_3$C–N–CH$_2$]	9.96
IE$_a$[H$_2$C–NH–CH$_2$ ring] to $^2A'$ H$_2$C–NH–CH$_2^+$ ring cation	9.33
IE$_v$[H$_3$C–N–CH$_2$ ring]	10.00
AE$_0$[CH$_3$–N–CH$_2^+$, $^2A'(C_s)$/H$_3$C–N–CH$_3$, $^2B_1(C_{2v})$]	10.52
AE$_0$[H$_2$C–NH–CH$_2^+$, $^2A'(C_s$ ring)/H$_3$C–N©H$_3$, $^2B_1(C_{2v})$]	11.25
IE$_a$[H$_2$C–N–CH$_2$] to $^1A_1$ cation	6.83
IE$_v$[H$_2$C–N–CH$_2$] to singlet surface	8.63
IE$_a$[H$_2$C–N–CH$_2$] to $^3A_2$ cation	9.45
IE$_v$[H$_2$C–N–CH$_2$] to triplet surface	10.29
IE$_a$[H$_2$C–N–CH$_2$ $^2B_1$ ring] to $^1A_1$ ring	12.20
IE$_v$[H$_2$C–N–CH$_2$ $^2B_1$ ring] to singlet surface	10.42
IE$_a$[H$_2$C–N–CH$_2$ $^2B_1$ ring] to $^3B_1$ ring	9.85
IE$_v$[H$_2$C–N–CH$_2$ $^2B_1$ ring] to triplet surface	10.57
IE$_a$[H$_3$C–N–CH $^2A'(C_s,1)$] to $^1A_1$ cation	6.23
IE$_v$[H$_3$C–N–CH $^2A'(C_s,1)$] to singlet surface	7.70
IE$_a$[H$_3$C–N–CH $^2A'(C_s,1)$] to $^3A'$ cation	10.90
IE$_v$[H$_3$C–N–CH $^2A'(C_s,1)$] to triplet surface	11.98
IE$_a$[H$_3$C–N–CH $^2A'(C_s,2)$] to $^1A_1$ cation	6.03
IE$_v$[H$_3$C–N–CH $^2A'(C_s,2)$] to singlet surface	7.69
IE$_a$[H$_3$C–N–CH $^2A'(C_s,2)$] to $^3A'$ cation	10.70
IE$_v$[H$_3$C–N–CH $^2A'(C_s,2)$] to triplet surface	11.07
AE$_0$[CH$_2$–N–CH$_2^+$, $^1A_1(D_{2d})$/H$_3$C–N–CH$_2$, $^1A'(C_s)$]	10.61
AE$_0$[CH$_3$–N–CH$^+$, $^1A_1(C_{3v})$/H$_3$C–N–CH$_2$, $^1A'(C_s)$]	10.40
AE$_0$[CH$_3$–C–NH$^+$, $^1A_1(C_{3v})$/H$_3$C–N–CH$_2$, $^1A'(C_s)$]	9.90

ciation event following 193 nm excitation.[1] The photofragment TOF spectra at $m/e = 43$, 42, and 15 (shown in Figs. 2–4) were fit by two recoil translational energy distributions, $P(E_T)$'s (shown in Fig. 5), corresponding to primary N–CH$_3$ bond fission. That these $P(E_T)$'s are identical to those used previously to fit the 200 eV electron impact data[1] illustrates that the translational energy release is independent of ionization technique, as it should be. The assignment of these distinct channels to the processes

$$N(CH_3)_3 + 193\,\text{nm} \rightarrow CH_3 + N(CH_3)_2(\tilde{X}\,^2B_1), \quad (1)$$

$$\rightarrow CH_3 + N(CH_3)_2{}^*$$

$$\rightarrow CH_3 + H_2C=NCH_3 + H, \quad (2)$$

is shown in the following sections. Additionally, here we suggest that the slow, unfit signal at $m/e = 42$ (Fig. 3) is a NC$_2$H$_4$ product arising from secondary dissociation:

J. Chem. Phys., Vol. 113, No. 8, 22 August 2000

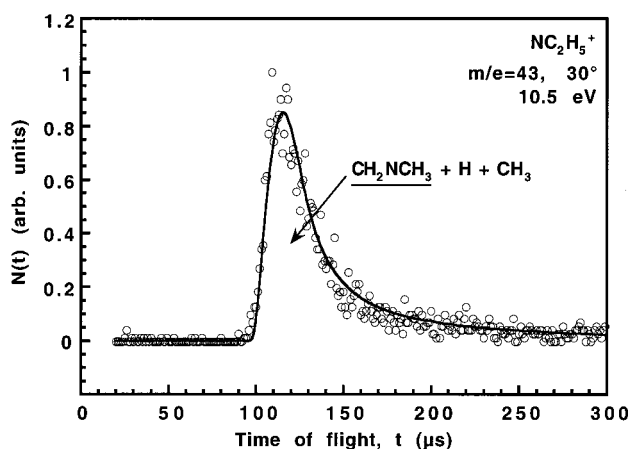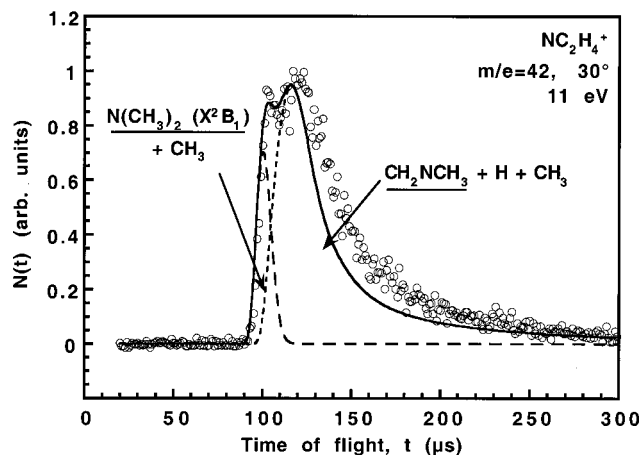Photodissociation of trimethylamine   3091

FIG. 2. The TOF spectrum of the products of trimethylamine photodissociation at 193 nm, recorded at $m/e = 43$, at a 30° source angle, and with 10.5 eV ionization energy. Experimental points are shown as open circles and the fit to the data is given as a solid line. The experimental data are fit beautifully by the same translational energy distribution $[P(E_T)]$ that was used previously (Ref. 1) to fit the signal observed at $m/e = 43$ following 200 eV electron-impact ionization of the photofragments of trimethylamine (see also Fig. 5).

$$N(CH_3)_3 + 193 \text{ nm} \rightarrow CH_3 + N(CH_3)_2^\dagger \rightarrow CH_3 + NC_2H_4 + H_2. \quad (3)$$

Photoion yield curves obtained by integrating photofragment TOF spectra at $m/e = 43$ and 42 (the only mass/charge ratios at which nitrogen-containing reaction products were observed in the present experiments) were used to characterize the products and are analyzed in the following sections. The results show that reactions (1)–(3) produce species with distinct photoionization characteristics. Because the reaction products also can be identified by kinetic energy release, we have determined that following 10.5 eV photoionization, the

FIG. 3. TOF spectrum of the products of trimethylamine photodissociation at 193 nm, recorded at $m/e = 42$, at a 30° source angle, and with 11 eV ionization energy. Experimental points are shown as open circles and the fit to the data is given as a solid line, with contributions from dissociation channels shown as broken lines. The fit uses the translational energy distributions $[P(E_T)$'s] determined previously from electron impact data (Ref. 1; see also Fig. 5), which leave the slow edge inadequately fit.
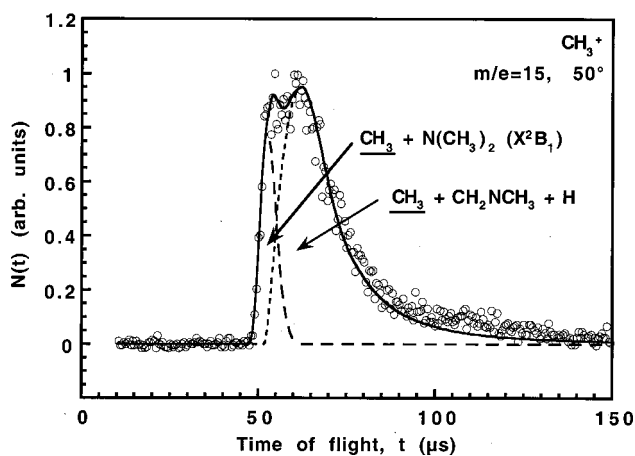

FIG. 4. A TOF spectrum of the products of trimethylamine photodissociation at 193 nm, recorded at $m/e = 15$, at a 50° source angle, and with 10.5 eV ionization energy. Experimental points are shown as open circles and the fit to the data is given as a solid line, with contributions from dissociation channels shown as broken lines. The fit uses the translational energy distributions $[P(E_T)$'s] determined previously from electron impact data (Ref. 1, see also Fig. 5).

nitrogen-containing products of reactions (1) and (3) appear at $m/e = 42$, while the nitrogen-containing product of reaction (2) appears at both $m/e = 43$ and $m/e = 42$. Additionally, each component of the TOF spectrum at $m/e = 42$ was found to have a distinct photoionization curve. Thus, each of the three distributions arises from a different neutral precursor.

A. Species appearing at $m/e = 43$: CH_2NCH_3

Although the photon resolution in these experiments is relatively low, the shape of the photoionization curve shown in Fig. 6 can be interpreted as representing the parent ionization of a species with a relatively broad Franck–Condon en-
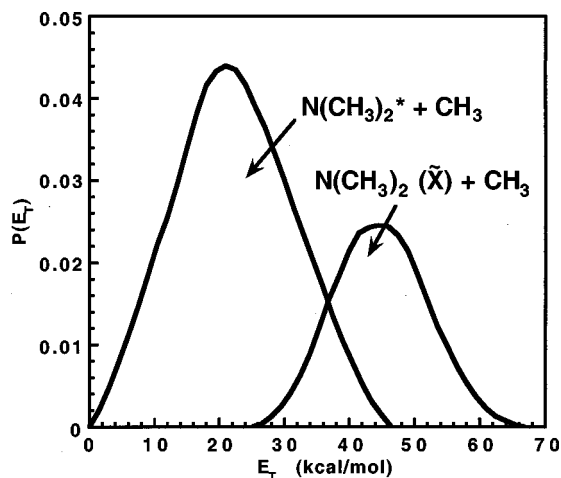

FIG. 5. Recoil translational energy distributions $[P(E_T)$'s] used to fit the TOF spectra both in this paper and in previous work (Ref. 1) that used 200 eV electron-impact ionization (Ref. 1). The faster $P(E_T)$, extending from 26–66 kcal/mol, was assigned previously (Ref. 1) to $N(CH_3)_2$ ($\tilde{X}\,^2B_1$) $+CH_3$. The slower $P(E_T)$ shown here, extending from 0–46 kcal/mol, corresponds to the primary formation of unstable $N(CH_3)_2^* + CH_3$, where the $N(CH_3)_2$ radical undergoes secondary H-atom loss prior to its arrival at the detector.
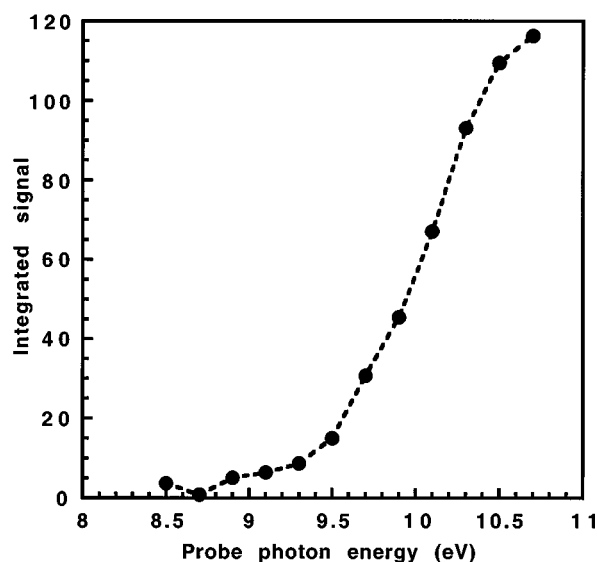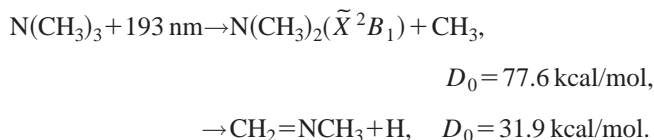
FIG. 6. Photoion yield curve for the species appearing at $m/e=43$. The TOF signal at $m/e=43$ was integrated from 96–300 μs, and the intensity shown in this plot has been corrected for variations in the probe photon flux. We have attributed this signal to the ionization of neutral CH_2NCH_3 secondary products.

velope, where the observed photoion spectral shape roughly corresponds to an integral over this envelope. The tail region hides unresolved initial (low) Franck–Condon factors, which, as the photon energy increases, build up and attain maximum probability in the region of steepest slope, finally leveling off when the Franck–Condon envelope is exhausted. If the final point in Fig. 6 represents a leveling off, then the vertical ionization energy of the species appearing at $m/e=43$ is close to $\sim$10.0 eV. Ideally, the signal onset at the low-energy end should correspond to the adiabatic ionization energy. However, the tail region is rendered complex by several factors, which tend to work in opposite directions: very low Franck–Condon factors tend to push the experimentally measurable onset to energies higher than the true adiabatic ionization energy, while low photon resolution and hot bands (arising from neutrals that are internally excited in the Franck–Condon active symmetric vibrational mode) tend to push the apparent onset toward lower energy. Selecting a point just before the more pronounced section of the ascent, such as $\sim$9.3 eV, should produce a relatively ''safe'' upper limit to the adiabatic ionization energy. The true adiabatic onset is expected to be in the ''tail'' region, at a lower energy and difficult to pinpoint more accurately.

Assuming the interpretation of the data at $m/e=43$ as parent ionization to be correct, then the neutral species in question has a composition NC_2H_5 with a vertical ionization energy of $\sim$10.0 eV and an adiabatic ionization energy of $<$9.3 eV. The simplest secondary dissociation process to produce NC_2H_5 from the primary $N(CH_3)_2$ product is straightforward C–H bond cleavage, leading to a $CH_3-N=CH_2$ structure. In agreement with this, we see in Table II that the adiabatic ionization energy $IE_a(CH_2=N-CH_3)=9.14$ eV and the vertical ionization energy $IE_v(CH_2=N-CH_3)=9.96$ eV at the G3 level of theory.

This reinforces the assignment of the neutral species to $CH_2=NCH_3$, $^1A'(C_s)$, formed by secondary dissociation of $N(CH_3)_2$ radicals:

$$N(CH_3)_3 + 193\ nm \rightarrow N(CH_3)_2(\tilde{X}\,^2B_1) + CH_3,$$

$$D_0 = 77.6\ kcal/mol,$$

$$\rightarrow CH_2=NCH_3 + H, \quad D_0 = 31.9\ kcal/mol.$$

The calculated minimum energy required for the secondary production of $CH_2=NCH_3$ is thus 109.5 kcal/mol (see Table V of Ref. 35), which corresponds to a maximum of 39 kcal/mol remaining for relative product translation. The less precisely determined experimental enthalpy changes are smaller for each reaction above, giving a maximum of 44 kcal/mol available for product translation. The translational energy distribution for this reaction, the slower one in Fig. 5, extends to 46 kcal/mol. The upper limit of this $P(E_T)$ is difficult to determine, however, because it assumes secondary H-atom loss from $N(CH_3)_2$ to have no impact on the velocity of the CH_2NCH_3 products. Within this assumption, the calculated and observed maximum translational energies are in quite reasonable agreement.

B. Shape and energetics of the TOF spectra at $m/e = 42$

The photofragment TOF spectrum at $m/e=42$ obtained by 11 eV photoionization (see Fig. 3) is very similar to that obtained using 200 eV electron impact ionization,[1] where the bulk of the signal is fit well with the two $P(E_T)$'s shown in Fig. 5. Because the translational energies of the fastest products extend close to the limit of available energy following N–CH$_3$ bond fission [compare $E_{avl}=70\pm3$ kcal/mol from G3 calculations with the maximum translational energy in the faster $P(E_T)$ in Fig. 5], the higher kinetic energy distribution is attributed to $N(CH_3)_2(\tilde{X}\,^2B_1)$ radicals formed with little internal energy, which arrive intact at the detector.[1] The slower $P(E_T)$ was assigned in the previous section to unstable $N(CH_3)_2*$ primary products that undergo secondary H-atom loss to CH_2NCH_3, appearing when ionized at both $m/e=43$ and $m/e=42$.

The shape of the $m/e=42$ TOF spectrum changes markedly at lower photoionization energy (see Fig. 7 obtained at 10 eV), where not only are the different ionization efficiencies of the contributing species obvious, but the rising edge of the spectrum is also overfit by the faster $P(E_T)$. The change in the rising edge is puzzling, as this indicates ionization of only a slow subset of the $N(CH_3)_2$ reaction products. It is possible that the ionization is dependent on the internal energy of the radicals, and that at 10 eV, the fastest $N(CH_3)_2(\tilde{X}\,^2B_1)$ products (i.e., those with the least internal energy) are not being ionized. The ionization efficiency of polyatomic radicals is not usually so strongly dependent on internal energy, however, and if this explanation is true, it would represent a rather unusual case.

Also apparent in Fig. 3 is additional slow TOF signal not fit by either of the $P(E_T)$'s shown in Fig. 5. A similarly underfit slow signal at $m/e=42$ was observed in the experiments utilizing 200 eV EI ionization.[1] (The scatter in the data
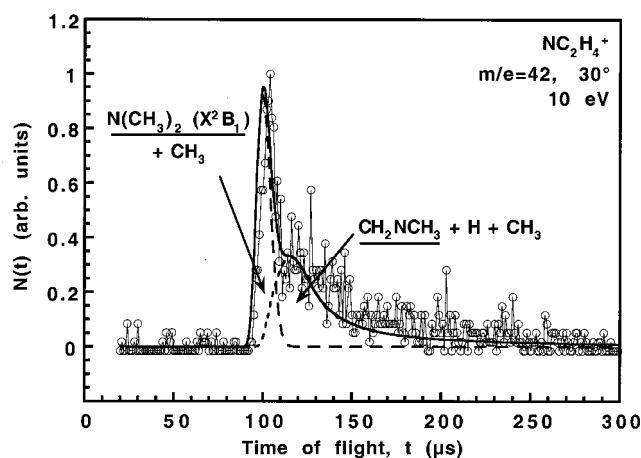
FIG. 7. TOF spectrum of the products of trimethylamine photodissociation at 193 nm, recorded at $m/e=42$, at a 30° source angle, and with 10 eV ionization energy. Experimental points are shown as open circles connected by thin lines, the fit to the data is given as a solid line, and contributions from dissociation channels are shown as broken lines. The fit uses the translational energy distributions [$P(E_T)$'s] determined previously from electron impact data (Ref. 1; also see Fig. 5). At this ionization energy, the TOF spectrum is bimodal, and the fit to the data appears to be too broad, especially for the fast peak. Reasons for this effect are discussed in the text.

points at lower ionization energies in Fig. 7 may obscure the need for an additional slow distribution to fit this signal as well.) $N(CH_3)_2$ and CH_2NCH_3 products contribute to the faster portion of the $m/e=42$ TOF signal; as there are no other obvious neutral products of mass 44 or 43, we consider secondary dissociation of $N(CH_3)_2 \rightarrow NC_2H_4 + H_2$ as a possibility.

In order to convert the observed unfit portion of the TOF distribution into a translational energy release distribution, there must be a TOF observation for the momentum-matched partner. Even if we assume H_2 loss to leave the velocity of the NC_2H_4 radicals unchanged from their $N(CH_3)_2$ parents (as would be the case in a barrierless process), there is no slow signal in the CH_3 TOF spectrum unfit by reactions (1) and (2) (see Fig. 4). This is not overly surprising, as it is likely that H_2 loss provides a velocity "kick" to the recoiling NC_2H_4 radicals, such that their times of arrival at the detector are broadened to fast and particularly to slow times compared to the methyl radicals that are momentum matched to the unstable $N(CH_3)_2^\dagger$ precursor. The best we can do then is to fit the slow portion of the $m/e=42$ TOF distribution to a velocity distribution, $P(v)$, of the neutral precursor to the signal at $m/e=42$, shown in Fig. 8.

If this distribution indeed corresponds to primary dissociation to unstable $N(CH_3)_2^\dagger + CH_3$, we can obtain a $P(E_T)$ by converting from velocity to recoil translational energy. The $P(E_T)$ thus derived extends from 0–24 kcal/mol and is likely broader than the "true" primary $P(E_T)$, due to the probable exit barrier to H_2 loss and concomitant velocity kick imparted to the NC_2H_4 radicals. The upper limit can be used to find the minimum internal energy of the unstable $N(CH_3)_2^\dagger$ radicals. The available energy following 193 nm excitation and N–CH_3 bond fission is given by $(148-78 =)70$ kcal/mol. The upper limit of the $P(E_T)$ derived from
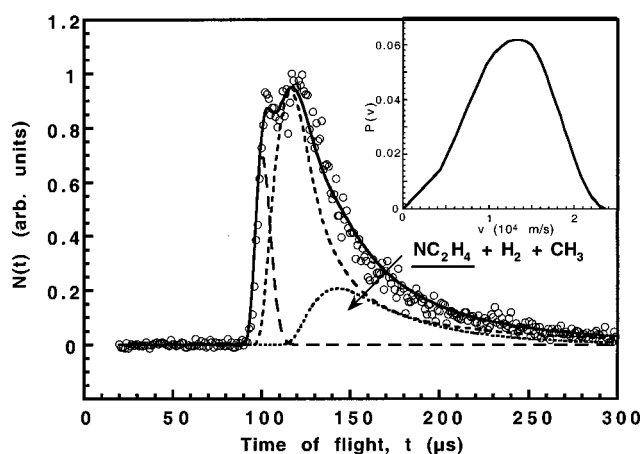

FIG. 8. An additional velocity distribution, $P(v)$, shown in the inset, can be used to fit the slowest, previously unfit portion of the signal at $m/e=42$. (The TOF data is the same as shown in Fig. 3.)

the $P(v)$ shown in Fig. 8 is 24 kcal/mol, corresponding to an internal energy of $N(CH_3)_2$ radicals of $(70-24 =)46$ kcal/mol, assuming the formation of internally cold CH_3 radicals. This value provides a very rough estimate of the energy required to undergo secondary H_2 loss from $N(CH_3)_2$.

Possible radical structures with chemical formula NC_2H_4 and the related enthalpies of reaction (at the G3 level of theory) are as follows:
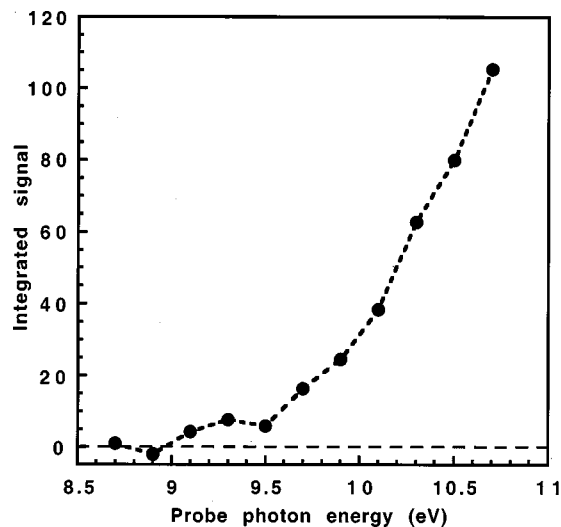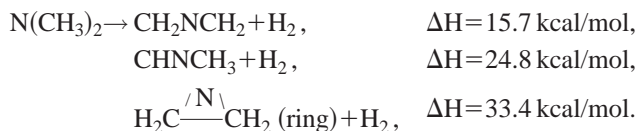
$$N(CH_3)_2 \rightarrow CH_2NCH_2 + H_2, \qquad \Delta H = 15.7 \text{ kcal/mol},$$
$$CHNCH_3 + H_2, \qquad \Delta H = 24.8 \text{ kcal/mol},$$
$$H_2C \overset{/N\backslash}{\underline{\qquad}} CH_2 \text{ (ring)} + H_2, \qquad \Delta H = 33.4 \text{ kcal/mol}.$$

FIG. 9. The total photoionization efficiency curve for all species appearing at $m/e=42$. The TOF signal at $m/e=42$ was integrated from 90–300 μs, and intensities have been corrected for variations in the probe photon flux. Three possible contributions can be seen in this plot, perhaps corresponding to the three distributions used to fit the $m/e=42$ TOF spectrum in Fig. 8. The ion signal starts to appear around 9.0–9.1 eV, and levels off after a modest increase. A second contribution starts at ~9.5 eV, and the third contribution commences at ~10.0–10.1 eV.

All of these possible structures are energetically accessible, and we now turn to the ion appearance energies at $m/e = 42$ for additional information that may help in identifying this species.

C. Ionization characteristics of the species appearing at $m/e = 42$: $N(CH_3)_2$, CH_2NCH_3, and NC_2H_4

The total photoion yield curve corresponding to $m/e = 42$, shown in Fig. 9, hints at three contributions that may correspond to the three distributions used to fit the $m/e = 42$ TOF spectra. The ion signal starts to appear around 9.0–9.1 eV, and, after a modest increase, quickly levels off. A second, slightly more pronounced contribution starts at ~9.5 eV, causing the ion yield to ascend nearly linearly until ~10.1 eV. At that point there appears to be a break in the slope, and a new, quasilinear increase in the ion yield ensues, continuing to the highest energy point recorded here. We have attempted to determine independently the partial photoion yield of each contribution, by integrating separately the signal over times of flight where each of the $P(E_T)$'s and $P(v)$ is dominant. Unfortunately, as seen in Fig. 8, the arrival times of the three components overlap to a great extent, making a clean separation of the three components difficult to achieve and resulting in ''cross-contamination.'' In addition, the three partial photoionization yield curves have significantly larger scatter than the total photoion yield curve, making the interpretation even more difficult.

Figure 10(a) shows the partial photoionization yield curve for the fastest signal at $m/e = 42$, obtained by integrating the time-of-flight signal between 90 and 100 μs. At the earliest of these flight times, only the fast channel contributes, and over the rest of this integration range, the relative intensity of the middle distribution is less than 10% of that of the fast distribution. The partial photoion yield has an apparent onset at ~9.1 eV, after which it curves up to ~10.2 eV, where it shows a tendency to level off. This is followed by a further increase given by a few scattered points at higher energies, although it is not entirely clear whether this belongs to the ''fast'' component or represents a ''contamination'' from the middle component. A comparison with the total yield in Fig. 9 suggests that the fastest component is predominantly responsible for the portion of the total yield at lowest energies.

The overall shape of the spectrum in Fig. 10(a) strongly suggests parent ionization, with an adiabatic ionization onset of ~9.1 eV (or lower) and a vertical ionization energy very roughly 0.6–0.7 eV higher. These values show excellent agreement with the predicted adiabatic and vertical ionization energies of CH_3NCH_3 (see Table II). The calculated adiabatic ionization energy of CH_3NCH_3 to the triplet cation of similar structure (dimethyl nitrenium) is predicted to be 9.0 eV, and to the singlet cation to be 9.1 eV, both coinciding with the discernible onset in Fig. 10(a). Furthermore, the predicted vertical ionization energies of dimethyl amidogen to the singlet and triplet ionic surfaces are 9.7 and 9.8 eV, respectively, quite close to the middle of the first rise in Fig. 10(a).

Figure 10(b) displays the partial photoionization efficiency curve associated with the ''middle'' species at m/e
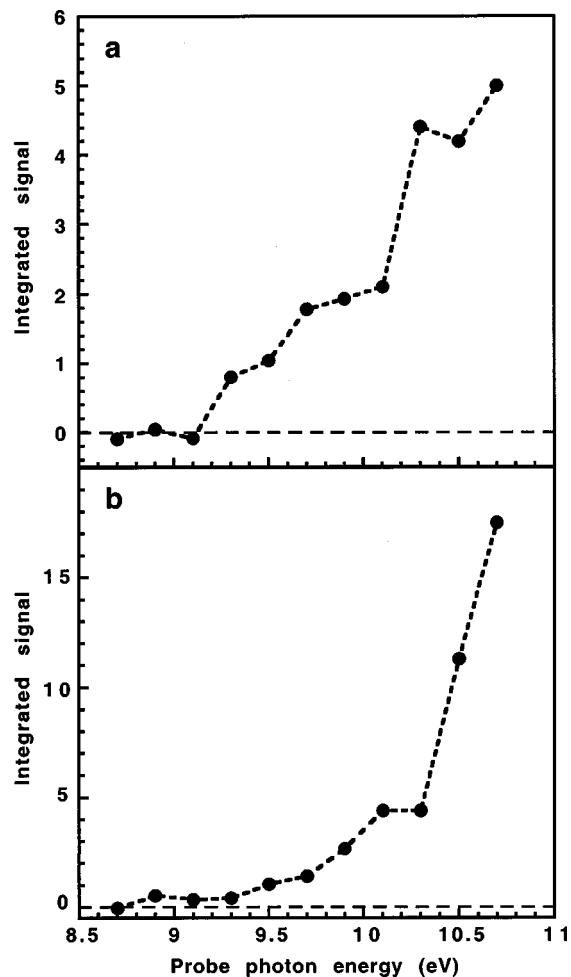

FIG. 10. The partial photoionization efficiency curve corresponding to the fastest two species appearing at $m/e = 42$. (a) Fastest species: The TOF signal at $m/e = 42$ was integrated from 90–100 μs, and the intensity shown in this plot has been corrected for variations in the probe photon flux. The spectrum can be attributed to neutral $N(CH_3)_2$ radicals, undergoing efficient dissociative ionization to $NC_2H_4^+$ fragment ions (see the text). (b) Middle species: The TOF signal at $m/e = 42$ was integrated from 112–121 μs, and the intensity shown in this plot has been corrected for variations in the probe photon flux. The spectrum can be attributed to dissociative ionization of CH_2NCH_3 (see the text).

$= 42$, obtained by integrating the photofragment TOF spectra between 112 and 121 μsec. While it is very difficult to avoid contributions from both the ''fast'' and the ''slow'' components, the integration limits chosen here are an attempt to minimize these unwanted contributions by keeping their sum to less than 10% of the desired ''middle'' component. The partial spectrum of the ''middle'' component seems to correspond to the rise seen at the high-energy end of the total photoionization efficiency spectrum presented in Fig. 9.

A fragment resulting from photodissociative ionization of a heavier parent is the most likely source of the signal in Fig. 10(b), judging by the general shape of the spectrum.[37,38] The quasilinear rise at higher energy suggests that the appearance energy for the fragment in question is in the neighborhood of 9.8–9.9 eV. (Technically, this value should be corrected for the average internal energy of the neutral parent, which may be available to the photodissociative ionization process. In the present case such a correction is rather

difficult to do reliably, and may not be particularly important, given the approximate nature of the extracted appearance energy and the expectation that the excess energy of the parent will not be particularly well randomized between the available internal modes.) The assignment of this middle species to CH_2NCH_3 is in agreement with calculations, which predict it to dissociatively ionize to the most stable isomer of $NC_2H_4^+$, N-protonated acetonitrile ($H_3C-C\equiv N^+-H$) at 9.9 eV (see Table IV of Ref. 35).

Finally, we focus our attention on the remaining ''slow'' species. Partial photoionization yield curves[35] suggest an ionization onset of ≤ 9.5 eV and a vertical ionization energy of ≥ 10.0 eV. The shape of the spectra suggests that the signal could arise from parent ionization, with two neutral species as obvious possibilities: CH_3NCH and CH_2NCH_2 [both arising from secondary dissociation of $N(CH_3)_2$]. The two species differ in the source of the secondary H_2 elimination, with the underlying assumption for facile production of either species that the transition state for elimination does not cause a skeletal rearrangement. Comparing the experimental with the calculated values in Table II, it seems most likely that the slow species is CH_2NCH_2 with ionization to the triplet surface ($IE_{ad}=9.4$ eV and $IE_{vert}=10.3$ eV). It is hard to explain why ionization of CH_2NCH_2 to the singlet surface of the ion is missing, unless (as witnessed by the large difference of 1.8 eV between the adiabatic and vertical ionization energy) this results in a very extended Franck–Condon envelope that corresponds to a weak feature not easily discernible above the background scatter.

A radical structure in which CH_2NCH_2 forms a ring is also a possibility. The apparent onset of ionization is lower than adiabatic ionization either to the $^3B_1$ ion (9.9 eV) or to the $^1A_1$ ion (10.2 eV), but this may be a result of the low-energy tail of the ''middle'' species, which is also present in the spectra. The vertical ionization energies to these surfaces (10.7 and 10.4 eV, respectively) show good agreement with the midpoint of the rise in photoion signal.[35] Hence, the assignment of the ''slow'' species as the CH_2NCH_2 ring structure cannot be excluded.

V. DISCUSSION AND SUMMARY

Under soft photoionization conditions at the Advanced Light Source, we have been able to identify several products of trimethylamine photodissociation at 193 nm. We have characterized the $N(CH_3)_2$ primary product and CH_2NCH_3 secondary product, and have set some energetic limits on another secondary product, perhaps corresponding to NC_2H_4.

The radical $N(CH_3)_2$ has an experimentally determined ionization onset of 9.1 ± 0.2 eV, which is interpreted as being close to its adiabatic ionization energy. The calculated adiabatic ionization energy at the G3 level is 9.0 ± 0.1 eV, similar to previous results at the G1 and G2 level (9.1 ± 0.1 eV) by Wright and Miller.[39] The experimental evidence presented here suggests that the $N(CH_3)_2^+$ ion formed by the photoionization of neutral $N(CH_3)_2$ is unstable and very efficiently fragments on the timescale of the experiment to produce an ion of $m/e=42$. This suggestion is reinforced by the obser-

vation that at all explored energies in these experiments, we were unable to observe $m/e=44$ beyond the limit of $<10^{-3}$ of the intensity at $m/e=43$. Hence, the parent ion of CH_3NCH_3 gives, at best, an extremely weak signal. Although the ionic species that is detected corresponds to a fragment, the onset and the shape of the photoionization efficiency curve are still defined by the Franck–Condon factors corresponding to the initial transition from the CH_3NCH_3 neutral to the $CH_3NCH_3^+$ surface(s). This is because a direct transition from the CH_3NCH_3 neutral to the $NC_2H_4^+ + H_2$ asymptote involves vanishingly small Franck–Condon factors, so does not contribute to the observable photoionization efficiency.

While G3 calculations do find a minimum corresponding to $CH_3NCH_3^+$ on both the singlet and triplet surfaces, they also show that the fragmentation of $CH_3NCH_3^+$ to $NC_2H_4^+ + H_2$ has several exothermic paths, depending on the assumed structure of the $NC_2H_4^+$ ion. For example, the most stable ion of the $NC_2H_4^+$ composition examined here, corresponding to N-protonated acetonitrile, $CH_3-C\equiv N-H, ^1A_1(C_{3v})$, corresponds to a fragmentation asymptote that is 51.7 kcal/mol downhill from the $CH_3NCH_3^+$ singlet ion.[35] The rearrangement required to access this asymptote is generally facile on ionic surfaces (usually much moreso than on neutral surfaces). A more exhaustive theoretical examination of the $NC_2H_4^+$ potential energy surfaces (at the MP2/6-31G(d)//4-31G level)[34] also found this ion to be the most stable structure on the singlet surface. The same study indicated that the lowest $NC_2H_4^+$ ion on the triplet surface is ~ 69 kcal/mol higher in energy, and hence does not provide an exothermic path for photodissociative ionization of dimethylamidogen on the triplet surface.

Although we have not tried to estimate the depth of the $CH_3NCH_3^+$ minimum in the G3 calculations, nor have we tried to identify the transition state that would lead to a $NC_2H_4^+ + H_2$ asymptote, prior theoretical studies indicate that the dimethylnitrenium ion is not particularly stable. For example, Ford and Herman[32] found that at the MP2(full)/6-31G(d) level the $CH_3NCH_3^+$ ion does not correspond to a local minimum on the singlet surface, but to a transition state for H migration to the immonium ion ($CH_2NHCH_3^+$), while on the triplet surface the nitrenium ($CH_3NCH_3^+$) and immonium ions were found to lie within 0.2 kcal/mol. For a comparison, at the G3 level of theory the immonium ion is also more stable than the nitrenium ion by 76.9 kcal/mol on the singlet surface, while on the triplet surface the immonium ion is less stable by 1.2 kcal/mol.[35]

Two studies in the literature have found a value of the ionization energy of CH_3-N-CH_3, which lies in close agreement with that reported here.[8,20] Those studies, however, relied on the pyrolysis of $(CH_3)_2NNO$[8,20] and $(CH_3)_2NNH_2$[8] to provide the $N(CH_3)_2$ radicals, a not particularly clean technique. It tends to produce a complex mixture of secondary species arising from equilibration to other isomers on the hot walls and recombination in the reaction vessel. Although Fisher and Henderson reported a signal at the parent ion ($m/e=44$), they also reported signals at $m/e=45$ and 43, interpreted as arising from ionization of dimethylamine, $NH(CH_3)_2$ and methylenemethylamine, $CH_3N=CH_2$.[8]

Hence, it is not clear *a priori* whether their signal at $m/e = 44$ corresponds to direct ionization of CH_3-N-CH_3, as they suggested, or to some other isomer resulting from equilibration on the wall. In fact, it is not even clear whether their signal at $m/e = 44$ arises from parent ionization or corresponds to dissociative ionization from a heavier species.

Castleman and co-workers[40] reported a lower (9.2 ± 0.2 eV) and upper (9.9 ± 0.2 eV) limit to the appearance energy of the fragmentation process:

$$NH(CH_3)_2 \rightarrow NC_2H_6^+ + H.$$
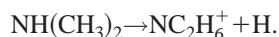
While the resulting ion has $m/e = 44$, they suggested that its structure is $CH_2NHCH_3^+$ rather than $CH_3NCH_3^+$. Indeed, using $\Delta H_{f,298}^0[NH(CH_3)_2] = -4.7 \pm 0.5$ kcal/mol[5] (0.5 ± 0.5 kcal/mol at 0 K) with the 9.2–9.9 eV range for the appearance energy, one obtains $\Delta H_{f,0}^0(NC_2H_6^+)$ in the range of 165 ± 5 to 175 ± 5 kcal/mol, very close to our calculated enthalpy of formation for the singlet ground state of $CH_2NHCH_3^+$ (see Table IV[35]). Other experiments (notably those of Levsen and McLafferty[41] and Thon *et al.*[42]) that sought an ion of structure $N(CH_3)_2^+$, observed no signal at $m/e = 44$ following 70 eV ionization. Thon *et al.* studied the thermal decomposition of trimethylamine, and found the intensity of their suspected $N(CH_3)_2$ primary product at $m/e = 44$ to be very low (below the error limit); however, the signal they observed at $m/e = 42$ was strong. (They made no mention of the signal at $m/e = 43$.) Levsen and McLafferty, who used collisional activation, characterized the decomposition of ions of formula $NC_2H_6^+$, produced from various sources, including trimethylamine. They found no peak at $m/e = 44$, and concluded that ions of initial structure $CH_3NCH_3^+$ rearrange to $CH_3NH=CH_2^+$ faster than the 10^{-5} s drift time in their experiments. Then, depending on the amount of internal excitation of the latter ion, H-atom or H_2 loss occurs, giving rise to the observed signals at $m/e = 43$ and $m/e = 42$. In addition, they noticed that high internal energies favor H loss, while low internal energies increase the H_2-loss channel. This seems to match our observation, where the fastest primary $N(CH_3)_2$ photoproducts (i.e., those with the least internal energy) appear only at $m/e = 42$, following H_2 loss in the ion. Our calculations show that the fragmentation of $N(CH_3)_2^+$ to $NC_2H_4^+ + H_2$ can be exoergic by ~ 50 kcal/mol, if the $NC_2H_4^+$ ion corresponds to the N-protonated acetonitrile, helping to explain how H_2 loss can occur, even from those $N(CH_3)_2$ radicals with very little internal energy. The lack of any parent signal at $m/e = 44$ at near-threshold photoionization conditions implies that this fragmentation has a very low barrier.

The CH_2NCH_3 closed-shell species formed in these experiments by secondary H-atom loss from $N(CH_3)_2$ has an experimentally determined ionization onset of <9.3 eV. The calculated adiabatic ionization energy is 9.1 eV, while the vertical ionization energy from internally cold CH_2NCH_3 is predicted to lie near 10 eV. A comparison with literature values places the experimental and adiabatic values toward the low end of previous observations[5] (ranging from 9.3–10.0 eV; see Table I), while the calculated vertical value is in agreement with the higher values, which also correspond to vertical ionization energies. In our experiments, the signal

from CH_2NCH_3 appears not only at its parent ion $m/e = 43$ but also as a fragment at $m/e = 42$. The calculated appearance energy for CH_3-C-NH^+ fragment ions of $CH_3NCH_2^+$ is 9.9 eV, while the experimentally observed onset (uncorrected for the effect of the internal energy excitation) is ~ 9.8–9.9 eV. The close agreement between these values, together with the agreement of our ionization onset with previous observations and calculations, support our assignment of the ''middle'' distribution to CH_2NCH_3 closed-shell species, formed by secondary dissociation of $N(CH_3)_2$ primary photoproducts.

Additionally, we have attempted to characterize the slowest species appearing at $m/e = 42$. It would appear that this slowest channel arises from an internally hot primary $N(CH_3)_2$ photofragment undergoing secondary H_2 loss. We were not able to study the H_2 molecule TOF distributions, and so this assignment is based solely on the inferred photoionization properties of the slowest signal at $m/e = 42$. A comparison of the photoion yield spectra (which suggest an ionization onset of 9.5–9.6 eV) with calculated adiabatic and vertical ionization energies does not allow us to definitively assign this species. Studies utilizing higher resolution photoionization will be of great assistance in better characterizing this species. Additionally, the paucity of information in the literature on nitrogen-containing radicals of formula NC_2H_4 leaves the results of the present study awaiting further experiments and calculations in order to definitively assign this species. The results of this work provide a starting point for future studies on the NC_2H_4 radical, while also providing new information on the dissociation dynamics of the primary $N(CH_3)_2$ radical products of the photodissociation of trimethylamine at 193 nm. The dissociation dynamics of nitrogen-containing systems have proven to be rich and complex, containing surprisingly unstable $N(CH_3)_2$ radicals, and provide a fertile ground for further studies.

[1] N. R. Forde, M. L. Morton, S. L. Curry, S. J. Wrenn, and L. J. Butler, J. Chem. Phys. **111**, 4558 (1999).

[2] N. R. Forde, T. L. Myers, and L. J. Butler, Faraday Discuss. **108**, 221 (1997).

[3] N. R. Forde, L. J. Butler, and S. A. Abrash, J. Chem. Phys. **110**, 8954 (1999).

[4] S. A. Abrash, D. M. Potts, and K. F. Freed, in preparation.

[5] H. Y. Afeefy, J. F. Liebman, and S. E. Stein, in *NIST Standard Reference Database Number 69*, edited by W. G. W. G. Mallard and J. P. Linstrom

(National Institute of Standards and Technology; http://webbook.nist.gov, Gaithersburg, MD, 1997).

[6] J. D. Cox and G. Pilcher, *Thermochemistry of Organic and Organometallic Compounds* (Academic, New York, 1970).

[7] D. D. M. Wayner, K. B. Clark, A. Rauk, D. Yu, and D. A. Armstrong, J. Am. Chem. Soc. **119**, 8925 (1997).

[8] I. P. Fisher and E. Henderson, Trans. Faraday Soc. **63**, 1342 (1967).

[9] Y. D. Orlov, E. A. Miroshnichenko, L. I. Korchatova, V. P. Vorobeva, and Y. A. Lebedev, Zh. Fiz. Khim. **70**, 1749 (1996).

[10] D. F. McMillen and D. M. Golden, Annu. Rev. Phys. Chem. **33**, 493 (1982).

[11] J. L. Franklin, J. G. Dillard, H. M. Rosenstock, J. T. Herron, K. Draxl, and F. H. Field, Natl. Stand. Ref. Data Ser. (U.S., Natl. Bur. Stand.) **26**, 95 (1969).

[12] B. G. Gowenlock, P. P. Jones, and J. R. Majer, Trans. Faraday Soc. **57**, 23 (1961).

[13] S. A. Lloyd, M. E. Umstead, and M. C. Lin, J. Energ. Mater. **3**, 187 (1985).

[14] J. L. Franklin and D. K. Sen Sharma, Adv. Mass Spectrom. **6**, 947 (1974).

[15] J. A. Kerr, Chem. Rev. **66**, 465 (1966).

[16] S. W. Benson and H. E. O'Neal, National Standards Reference Data Service, NBS, Washington, DC, 1970, Vol. 21.

[17] D. M. Golden, R. K. Solly, N. A. Gac, and S. W. Benson, J. Am. Chem. Soc. **94**, 363 (1972).

[18] R. A. L. Peerboom, S. Ingemann, N. M. M. Nico, and J. F. Liebman, J. Chem. Soc., Perkin Trans. 2, 1825 (1990).

[19] Y. G. Lazarou and P. Papaginnakoupulos, J. Phys. Chem. **97**, 4468 (1993).

[20] Q. Chunhua, H. Gongyi, and W. Dianxun, J. Phys. Chem. **103**, 1972 (1999).

[21] D. M. Golden (personal communication, 1999).

[22] X. Yang, J. Lin, Y. T. Lee, D. A. Blank, A. G. Suits, and A. M. Wodtke, Rev. Sci. Instrum. **68**, 3317 (1997).

[23] P. A. Heimann, M. Koike, C. W. Hsu *et al.*, Proc. SPIE **2856**, 90 (1996).

[24] P. A. Heimann, M. Koike, C. W. Hsu *et al.*, Rev. Sci. Instrum. **68**, 1945 (1997).

[25] M. J. Frisch, G. W. Trucks, H. B. Schlegel *et al.*, GAUSSIAN 98 (Gaussian, Inc., Pittsburgh, PA, 1998).

[26] S. Hammerum and T. I. Solling, J. Am. Chem. Soc. **121**, 6002 (1999).

[27] J. Henricksen and S. Hammerum, Int. J. Mass Spectrom. **179**, 301 (1998).

[28] W. B. Tzeng, K. Narayanan, G. C. Chang, W. C. Tsai, and J. J. Ho, J. Phys. Chem. **100**, 15340 (1996).

[29] W. Koch and G. Frenking, J. Phys. Chem. **91**, 49 (1987).

[30] M. B. Seasholtz, T. B. Thompson, and N. G. Nelson, J. Phys. Chem. **99**, 17838 (1995).

[31] S. A. Shaffer, F. Turecek, and R. L. Cerny, J. Am. Chem. Soc. **115**, 12117 (1993).

[32] G. P. Ford and P. S. Herman, J. Am. Chem. Soc. **111**, 3987 (1989).

[33] V. Barone, F. Lelj, P. Grande, and N. Russo, Theochem **25**, 319 (1985).

[34] E.-U. Wurthwein, J. Org. Chem. **49**, 2971 (1984).

[35] See EPAPS Document No. E-JCPSA6-113-013032 for more details of the calculations performed here. This document may be retrieved via the EPAPS homepage (http://www.aip.org/pubservs/epaps.html) or from ftp.aip.org in the directory /epaps/. See the EPAPS homepage for more information.

[36] L. A. Curtiss, K. Raghavachari, P. C. Redfern, V. Rassolov, and J. A. Pople, J. Chem. Phys. **109**, 7764 (1998).

[37] P. M. Guyon and J. Berkowitz, J. Chem. Phys. **54**, 1814 (1971).

[38] W. A. Chupka, J. Chem. Phys. **54**, 1936 (1971).

[39] T. G. Wright and T. A. Miller, J. Phys. Chem. **100**, 4408 (1996).

[40] S. W. Sigsworth, R. G. Keesee, and A. W. Castleman, J. Am. Chem. Soc. **110**, 6682 (1988).

[41] K. Levsen and F. W. McLafferty, J. Am. Chem. Soc. **96**, 139 (1974).

[42] A. Thon, D. Saulys, S. A. Safvi, D. F. Gaines, and T. F. Kuech, J. Electrochem. Soc. **144**, 1127 (1997).

Characterization of Nitrogen-Containing Radical Products from the Photodissociation of Trimethylamine using Photoionization Detection

Supplementary Material

Nancy R. Forde and Laurie J. Butler
The James Franck Institute and Department of Chemistry
University of Chicago, Chicago, IL 60637

Branko Ruscic
Chemistry Division, Argonne National Laboratory, Argonne, IL 60439

Osman Sorkhabi, Fei Qi and Arthur Suits
Chemical Sciences Division, Lawrence Berkeley National Laboratory, Berkeley, CA 94720

Additional Details of G3 Calculations Presented in the Paper – See Also Tables III-V

Just as the earlier Gn calculations, the unmodified G3 sequence (which was used here) starts by optimizing the initial geometry and calculating vibrational frequencies at the HF/6-31G(d) level, followed by re-optimizing the geometry at the MP2(Full)/ 6-31G(d) level. The MP2 geometry is then used to perform the remaining calculations, which in the case of G3 are QCISD(T)/6-31G(d), MP4/6-31+G(d), MP4/6-31G(2df,p), and MP2(Full)/G3Large. These lead to an estimate of the total electronic energy that is effectively at the QCISD(T,full)/G3Large level. The final G3 total electronic energy is then obtained by including small empirical "higher level" corrections.

Within the G3 procedure, the role of the initial HF calculations is simply to provide the first step in the geometry optimization and yield vibrational frequencies that are used to estimate the zero-point vibrational energy. However, these frequencies are also used as an indicator of whether the proposed geometry corresponds to a true local minimum or a saddle point on the potential energy surface. Of the various structures examined here, ~1/3 appeared to belong to local minima, while ~2/3 corresponded to first or second order saddle points at the HF level. However, at least in principle, the subsequent MP2 optimization may drift away from the initial HF geometry, resulting in a G3 calculation for a different conformer or isomer. In addition, a geometry that corresponds to a stable minimum at the HF level, may correspond to a saddle point at the MP2 level and vice versa. In order to avoid such surprises, the majority of structures, whether corresponding to true minima or saddle points with one or more imaginary frequencies at the HF level, were rechecked by performing a geometry optimization and computation of frequencies at the B3LYP/6-311G(d,p) level of theory.[1-3] In general, the additional B3LYP calculations confirmed the G3 findings based on the HF and MP2 optimizations. With one exception, only species corresponding to true minima both at the HF/6-31G(d) and B3LYP/6-311G** levels are reported in Tables III-IV.

Description of Deconvolution of "Slowest" Component in *m/e*=42 Photoion Yield Determinations – See Figure 11

Unfortunately, as seen in Figure 8, over its entire range of TOF arrival times, signal from the "slow" species is overlapped by signal from the "middle" species. In order to minimize the contributions from the "middle" species, the TOF signal was integrated from 155-198 μsec, which corresponds to the range of arrival times at which the "slow" species contributes to 50±5 % of the total signal. The result is shown in Figure 11a. Taking into account that the spectrum really corresponds to a superposition of two species, its shape suggests that the "slow" species is probably responsible for the feature in the center of the total photoion efficiency curve presented in Figure 9. To further reduce contamination by the "middle" species, one can subtract its contribution from the photoion yield spectrum shown in Figure 10b. By scaling the "middle" photoion yield curve (Figure 10a) by the ratio of intensities under the middle-fit TOF curve used to obtain Figures 10a and 10b (area under 155-198 μs : area under 112-121 μs), the contribution of the middle species can be reduced, giving a clearer indication of the photoion yield spectrum of the slowest species at *m/e*=42. The result is shown in Figure 11b.

The scatter in the data in Figure 11b and the composite nature of the spectrum in Figure 11a permit only a tentative assignment of the source of the

slow TOF signal.   While far from unambiguous, the overall shape of these spectra suggests that the underlying photoionization process could be parent ionization of a species with a rather broad Franck-Condon envelope.   The apparent onset is ~9.5-9.6 eV, while the presumed vertical ionization is quite difficult to extract, although is not likely to be lower than ~10.0 eV.   Given the scatter in the data, a much lower (but weaker) ionization onset cannot be excluded. If the interpretation of the spectrum in Figure 11b as parent ionization at m/e=42 is correct, than there are two neutral species that appear as plausible candidates, based on the assumption that they originate via secondary dissociation of the primary $N(CH_3)_2$ photodissociation product: CH_3NCH and CH_2NCH_2.

Table III – Calculated enthalpies of formation of selected neutral species of interest to the present study. The values were obtained at the G3 level of theory and are listed at 0 K, with equivalent values at 298 K given in parentheses.

Species	Calculated Enthalpy of Formation at 0 K (298 K), kcal/mol	Remark
$N(CH_3)_3$, $^1A_1$ (C_{3v})	0.9 (-5.9)	
$CH_2N(CH_3)_2$, $^2A'$ (C_s)	40.4 (34.7)	
$H_3C-N-CH_3$, $^2B_1$ (C_{2v})	42.6 (38.6)	a
$H_2C-NH-CH_3$, ^2A (C_1)	40.2 (36.5)	
$H_3C-N-CH_2$, $^1A'$ (C_s)	22.9 (19.4)	b
$H_3C-N-CH_2$, $^3A''$ (C_s)	87.0 (83.8)	c
$H_2C-NH-CH_2$, $^1A'$ (C_s ring)	35.4 (31.4)	
$H_2C-N-CH_2$, $^2A_2$ (C_{2v})	58.3 (55.7)	d
$H_2C-N-CH_2$, $^2B_1$ (C_{2v} ring)	76.l (73.1)	e
$H_3C-N-CH$, $^2A'$ (C_s, *1*)	67.4 (64.9)	f
$H_3C-N-CH$, $^2A'$ (C_s, *2*)	72.0 (69.5)	g

a C_{2v} structure with a bent CNC frame, where on both sides one of the HCNC dihedral angles is 180˚

b   a C_s structure with a bent CNC frame, where on the CH_3 side one of the HCNC dihedral angles is 0˚, while on the CH_2 side one of the HCNC dihedral angles is 0˚ and the other is 180˚

c   a C_s structure with a bent CNC frame, where on the CH_3 side one of the HNCN dihedral angles is 0˚, while the CH_2 moiety is perpendicular to the CNC plane.

d   planar C_{2v} structure with a bent CNC frame, where on both sides one of the HCNC dihedral angles is 0˚ and the other is 180˚.

e   ring C_{2v} structure

f   a C_s structure with a bent CNC frame, where on the CH side the HCNC dihedral angle is 180°, while on the CH_3 side one of the HCNC dihedral angles is 0°

g   a C_s structure with a bent CNC frame, where on the CH side the HCNC dihedral angle is 0°, and on the CH_3 side one of the HCNC dihedral angles is also 0°

Table IV – Calculated enthalpies of formation of selected ionic species that are of interest to the present study. The values were obtained at the G3 level of theory and are listed at 0 K, with equivalent values at 298 K given in parentheses. The enthalpies of formation of ions follow the stationary electron convention (Ref. [4]).

Species	Calculated Enthalpy of Formation at 0 K (298 K), kcal/mol	Remark
$N(CH_3)_3^+$, $^2A''$ (C_{3h})	182.3 (176.2)	
$H_3C\text{-}N\text{-}CH_3^+$, $^3B_1$ (C_{2v})	249.4 (245.7)	a
$H_3C\text{-}N\text{-}CH_3^+$, ^1A (C_2)	251.4 (247.2)	b
$H_2C\text{-}NH_2\text{-}CH_2^+$, $^1A_1$ $(C_{2v}$ ring$)$	185.5 (180.6)	
$H_2C\text{-}NH\text{-}CH_3^+$, $^1A'$ (C_s)	174.5 (170.1)	c
$H_2C\text{-}NH\text{-}CH_3^+$, ^3A (C_1)	250.6 (246.8)	
$H_3C\text{-}N\text{-}CH_2^+$, $^2A'$ (C_s)	233.6 (230.6)	d
$H_2C\text{-}NH\text{-}CH_2^+$, $^2A'$ $(C_s$ ring$)$	250.6 (246.8)	
$H_2C\text{-}N\text{-}CH_2^+$, $^1A_1 (D_{2d})$	215.9 (213.3)	e
$H_2C\text{-}N\text{-}CH_2^+$, $^3A_2 (C_{2v})$	276.1 (273.7)	f
$H_2C\text{-}N\text{-}CH_2^+$, $^1A_1 (C_{2v}$ ring$)$	311.3 (308.6)	g
$H_2C\text{-}N\text{-}CH_2^+$, $^3B_1 (C_{2v}$ ring$)$	303.3 (300.5)	g
$H_3C\text{-}N\text{-}CH^+$, $^1A_1$ (C_{3v})	211.0 (208.5)	h
$H_3C\text{-}N\text{-}CH^+$, $^3A''$ (C_s)	331.0 (328.7)	i
$H_3C\text{-}N\text{-}CH^+$, $^3A'$ (C_s)	318.8 (316.5)	j
$H_3C\text{-}C\text{-}NH^+$, $^1A_1$ (C_{3v})	199.6 (197.1)	k

H$_2$C-C-NH$_2$$^+$, ^{1}A$_1$ (C$_{2v}$)	215.3 (212.7)	l

a   C$_{2v}$ structure with a bent CNC frame, where on both sides one of the HCNC dihedral angles is 180˚

b   a C$_2$ structure where on each side one of the HCNC dihedral angles is ~7˚; at the B3LYP level this corresponds to a C$_{2v}$ structure where the two dihedral angles are 0˚

c   a C$_s$ structure with a bent CNC frame, where the CH$_2$ and NH moieties and one of the H atoms on the CH$_3$ moiety (*trans* to the H atom on N) are in the CNC plane

d   a C$_s$ structure with a bent CNC frame, where on the CH$_3$ side one of the HCNC dihedral angles is 0˚, while on the CH$_2$ side one of the HCNC dihedral angles is 0˚ and the other is 180˚

e   a D$_{2d}$ structure with a linear CNC frame, where the two CH$_2$ moieties are perpendicular to each other

f   planar C$_{2v}$ structure with a bent CNC frame, where on both sides one of the HCNC dihedral angles is 0˚ and the other is 180˚.

g   ring C$_{2v}$ structure

h   a C$_{3v}$ structure with a linear CNCH frame

i   a C$_s$ structure with a bent CNC frame, where on the CH side the HCNC dihedral angle is 180˚, while on the CH$_3$ side one of the HCNC dihedral angles is 0˚

j   a C$_s$ structure with a bent CNC frame, where on the CH side the HCNC dihedral angle is 0˚, and on the CH$_3$ side one of the HCNC dihedral angles is also 0˚

k   a C$_{3v}$ structure with a linear CCNH frame

l   a C$_{2v}$ structure with a linear CCN frame with the NH$_2$ and CH$_2$ moieties in perpendicular planes

Table V – Calculated bond dissociation energies of interest to the present study. All values were calculated at the G3 level of theory at 0 K, with equivalent values at 298 K listed in parentheses.

Quantity	Calculated Value at 0 K (298 K)	Remark
$N(CH_3)_3 \rightarrow CH_2N(CH_3)_2 + H$	91.2 (92.7)	
$N(CH_3)_3 \rightarrow CH_3\text{-}N\text{-}CH_3 + CH_3$	77.6 (79.6)	a, b
$N(CH_3)_3 \rightarrow CH_2\text{-}NH\text{-}CH_3 + CH_3$	75.2 (77.4)	a, c
$CH_3\text{-}N\text{-}CH_3 \rightarrow CH_2\text{-}N\text{-}CH_3 + H$	31.9 (32.9)	
$CH_3\text{-}N\text{-}CH_3 \rightarrow CH_2\text{-}N\text{-}CH_2 + H_2$	15.7 (17.1)	
$CH_3\text{-}N\text{-}CH_3 \rightarrow CH_3\text{-}N\text{-}CH + H_2$	24.8 (26.3)	
$CH_3\text{-}N\text{-}CH_3 \rightarrow H_2C\underset{\cdot N^{\cdot}}{\quad}CH_2 + H_2$	33.4 (34.5)	

a $\Delta H^o_{f0}(CH_3) = 35.86\pm0.07$ kcal/mol from Ref. [5].
b   direct bond breakage to $^2B_1$ dimethyl amidogen
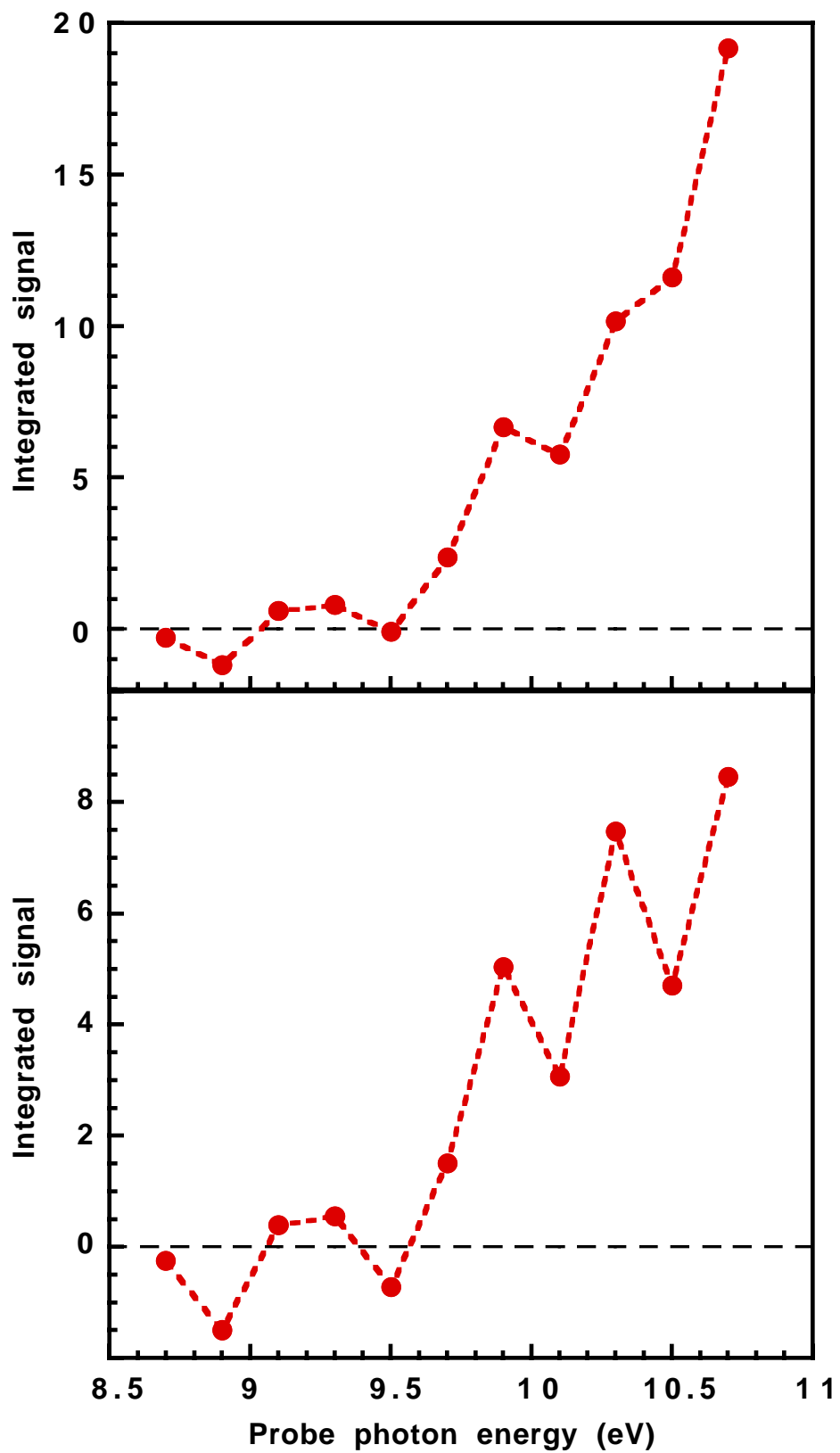c   requires rearrangement

Figure 11 - Partial photoionization efficiency curves corresponding to a superposition of the slowest and middle species appearing at *m/e*=42. (a) The TOF signal at *m/e*=42 was integrated from 155-198 μsec, and the intensity shown in this plot has been corrected for variations in the probe photon flux. (b) This curve was obtained by subtracting from (a) the photoion yield of the middle species at *m/e*=42 from 155-198 μsec (obtained by scaling Figure 10b by the ratio of area under the middle fit TOF curve from 112-121 μsec to the area from 155-198 μsec). This spectrum can be tentatively attributed to neutral NC_2H_4 radicals, formed from secondary dissociation of $N(CH_3)_2$ (see main text).

References

[1]   A. D. Becke, *J. Chem. Phys.* **98,** 5648 (1993).

[2]   C. Lee, W. Yang, and R. G. Parr, *Phys. Rev. B* **37,** 785 (1988).

[3]   B. Miechlich, A. Savin, H. Stoll, and H. Preuss, *Chem. Phys. Lett.* **157,** 200 (1989).

[4]   H. M. Rosenstock, in *Kinetics of Ion-Molecule Reactions*, edited by P. Ausloos (Plenum, New York, 1979), pp. 246.

[5]   B. Ruscic, M. Litorja, and R. L. Asher, *J. Phys. Chem. A* **103,** 8625 (1999).